Design, Construction and Validation of a Guarded Hot Plate Apparatus for Thermal Conductivity Measurement of High Thickness Crop-Based Specimens

Samuel DUBOIS*[1], Frédéric LEBEAU[1]

[1]Dept. STE, Gembloux Agro-Bio Tech, University of Liege, Belgium

*Corresponding author, supported by a F.R.I.A Grant,

Address: Dept. of environmental sciences and technologies, Gembloux Agro-Bio Tech, 2 Passage des déportés, 5030 Gembloux, Belgium (s.dubois@doct.ulg.ac.be)

KEYWORDS

Thermal Conductivity, Guarded Hot Plate, Crop-based materials, Straw bale

STATUS

Published in:

Materials and structures, 2013

ABSTRACT

The search for sustainability achievement in the building sector led to the use of crop-based insulation materials. Among these, raw products like plant straws bales can present elementary representative volumes (REVs) in the size order of several square centimeters. Fibers orientation may play an important role on material thermal behavior. Measuring their thermal conductivities with standard steady-state equipment can thus lead to some inaccuracies due to the necessity of resetting lower thickness samples. This paper presents a Guarded Hot Plate (GHP) apparatus designed to test high thickness samples, up to 40cm, with an accuracy of 2%. The different parts of the machine are described in details along with design process and challenges encountered. Temperature and heat flux measurements in the device represent critical design stages where optimal accuracy is needed in order to optimize the resulting global error. Regarding this, necessary numerical and experimental analyzes were conducted emphasizing on intrinsic systematic error assessment. To complete the study, some validations tests are performed on a reference material and other widely-spread polystyrene slabs. These tests take into account the optimal computation parameters resulting from the numerical analysis and the apparatus proved to be in accordance with accuracy requirements.

1. INTRODUCTION

The determination of the thermal conductivity of building materials is fundamental for solving problems related to building performance and user comfort. A variety of organic insulation products have been recently promoted for their sustainability, which includes crop-based materials [1, 2]. Among these some require a great thickness of implementation, either because their very nature requires it, like for straw bales construction [3-5], or to compensate for their lower thermal conductivity relatively to high performance inorganic insulation materials. There are many methods for measuring the thermal conductivity of materials, both in steady state and transient conditions. The stationary methods such as the so-called 'guarded hot plate technique' require thermal equilibrium and thus a significant measurement time. The boundary conditions imposed on the sample need also to be controlled precisely. However, if these boundary conditions are met, the results obtained by these methods are often very accurate [6]. The transient methods provide generally faster results and can be used on smaller samples but at the cost of lower accuracy.

The work presented here was directed towards the conception of an apparatus for thermal conductivity measurement in steady state, capable of performing over a wide range of thickness. More specifically it's expected to provide reliable results on an entire straw bale. This would be particularly useful to assess the effect of actual straws particles orientation in the bale on final thermal conductivity. This information might be particularly relevant for producers targeting the construction sector.

Much research has already been conducted on the thermal conductivity of straw bales. The effect of the direction of heat flow relatively to fibers orientation has already been highlighted [7-9]. It is accepted that the more the flow is parallel to the fibers, the greater the thermal conductivity. It is important to note however that most of available data drives either from transient methods [10], from steady-state methods performed on lower thickness re-built bales [11] or from compressed loose material [12, 13]. Absolute thermal conductivity measurements on an entire two-wired straw bale are thus still missing. The rearrangement of the samples often observed in literature for steady-state measurement is required by the low thickness generally imposed by commercial guarded-hot plate or heat flow meter apparatus. As the straw particle length can generally extend to 50cm [14], resetting lower thickness samples from original bale could lead to changes in structure the impact of which is hard to quantify.

The guarded hot plate prototype presented here allows measurements on thick specimens and offers the possibility to assess the thermal conductivity of non-altered straw bales samples. The approach is thus complementary to existing data. It offers the possibility of direct and easy comparison of bales from different origins or manufacturing. The original device is described in this paper along with particular design details and challenges encountered. Its performance will be assessed by performing the necessary numerical and experimental tests.

2. GUARDED HOT PLATE METHOD

2.1 General principle

The guarded hot plate (GHP) apparatus is traditionally recognized as the only absolute method for thermal conductivity measurement in steady-state of homogeneous materials able to achieve a global measurement uncertainty below 2% [6]. Its principle is to reproduce the uniform, unidirectional and constant thermal flux density existing through an infinite homogeneous slab-shaped specimen caught between two infinite isothermal planes. The method is defined in an international standard under the designation 'Thermal insulation - Determination of steady-state thermal resistance and related properties - Guarded hot plate apparatus' [15].

The device developed in this research is based on the 'single specimen apparatus' (**Fig. 1**). Their principle is the following: the analyzed specimen is sandwiched between an electrically-heated hot plate maintained at temperature T_h and a cold plate maintained at a lower temperature T_c. The heat dissipated by the Joule effect in the hot plate would travel to the cold plate through the sample, but also backwards and laterally on the edges of the hot plate. Back and lateral 'guard zones' are then necessary to neutralize these leaks. By maintaining the different guard zones at the same temperature T_h with precise control, all unwanted thermal transfers are indeed canceled. The hot plate is thus separated in two parts: a heater zone (or measurement zone) of known area and heated electrically and an adjacent guard ring heated with a different circuit. A small gap separates the two zones and a thermopile is often used to control the temperature difference between these. The back face of the hot plate is provided with an additional guard plate with identical dimensions providing protection from backwards thermal fluxes. This back guard plate also has its own heating system and is associated with appropriate temperature differential control as in lateral gap.

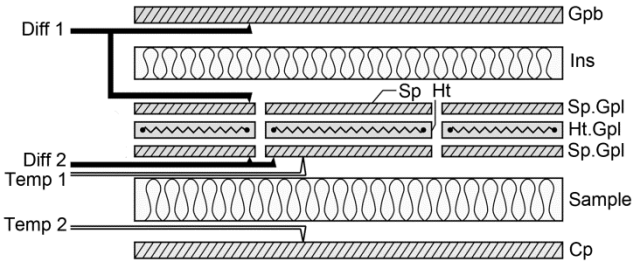

Cp : Cold plate
Diff 1 : Imbalance sensing element 1
Diff 2 : Imbalance sensing element 2
Gpb : Back guard plate
Ht : Measurement zone heating element
Ht.Gpl : Lateral guard heatin element
Ins : Thermal insulation
Sp : Measurement zone surface plate
Sp.Gpl : Lateral guard surface plate
Temp 1 : Temperature sensor 1
Temp 2 : Temperature sensor 2

Fig. 1. Single specimen GHP

When working well, with all three elements at exactly the same temperature T_h, the heat produced in the measurement plate will flow unidirectionally towards the cold plate. All the

others heat fluxes are supposed to be eliminated. With such device, the thermal conductivity is obtained by the one-dimensional Fourier equation:

$$\lambda = \frac{\Phi e}{A(T_h - T_c)} \tag{1}$$

Where Φ (W) is the heat flow-rate that in an ideal unidirectional condition would traverse the specimen through an area A (m^2) called measurement area. The variable e (m) is the thickness of the specimen. It's important to notice that the thermal flux Φ is equal to the electric power injected in the heater plate only if the instrument is perfect. For low thicknesses of samples the measurement area is considered approaching the surface bounded by the edge of the measurement plate. When using thick samples this area tends to the surface delimited by the line passing through the center of the gap. Generally the thermal conductivity value deduced is related to the average temperature of the tests T_m (**Equation 2**).

$$T_m = (T_h + T_c) / 2 \tag{2}$$

2.2 Chosen measurement approach

Figure 2 shows the schematic diagram of the GHP prototype presented here and highlights the differences in measurement strategy in comparison to a typical single specimen apparatus (**Fig. 1**). We will used what is referred as a 'hybrid method' [16] to obtain the heat flux Φ crossing the specimen, similarly to the device developed in [17]. The lateral and back guard plates are combined into a single massive metallic piece, called simply the guard (or hot) plate, and circulating water passing through tubes and thermal diffusers is used to maintain it at the temperature T_h. The measurement plate is incorporated in the center of this guard plate and electrically-heated. A heat flux meter (HFM) is sandwiched between the unique guard plate and the heater and allows to control precisely the temperature difference between the two pieces. **Figure 3** presents more precisely the principle of the hybrid method with the different heat fluxes involved.

At steady state the heat balance on the heater plate gives:

$$P_e = \Phi + \underbrace{\Phi_{gb} + \sum_{i=1}^{4} \Phi_{gl,i} + \sum_{i=1}^{4} \Phi_{edge,i}}_{\text{Parasite heat fluxes}} \tag{3}$$

$$P_e = \Phi + \Phi' \tag{4}$$

Where P_e is the electric power dissipated in the electric resistive circuit, Φ is the heat flux actually passing through the sample, $\sum_{i=1}^{4} \Phi_{gl,i}$ the heat flow passing to the guard plate laterally through the gap, Φ_{gb} the back heat flux going to the guard plate through the HFM and

$\sum_{i=1}^{4} \Phi_{edge,i}$ the edge loss, i.e. the heat produced by the heater that derives from the ideal vertical flow orientation and leave the sample through its edges. All these 'leak' fluxes depend on the temperature difference between the guard plate and the heater plate as well as the temperature of the edge of the sample during the test. When the temperature is the same in the guard and measurement plate and the edge of the sample is well insulated or far enough from the heater plate, it can be assumed that all the electrical power dissipated in the heater flows vertically through the sample, i.e. $P_e \cong \Phi$. In appropriate designs, Φ' is typically less than 0.5% of Φ [15].

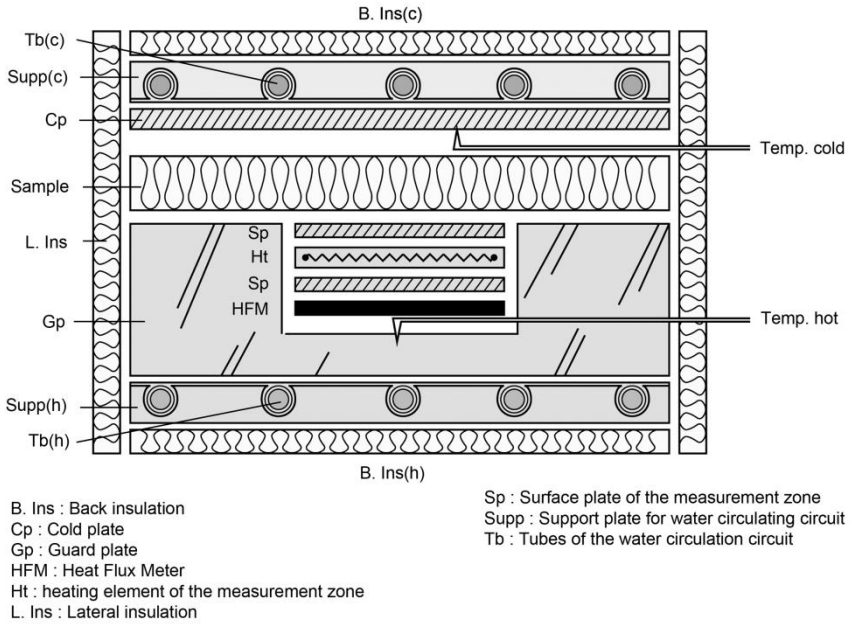

Fig. 2. Measurement principle

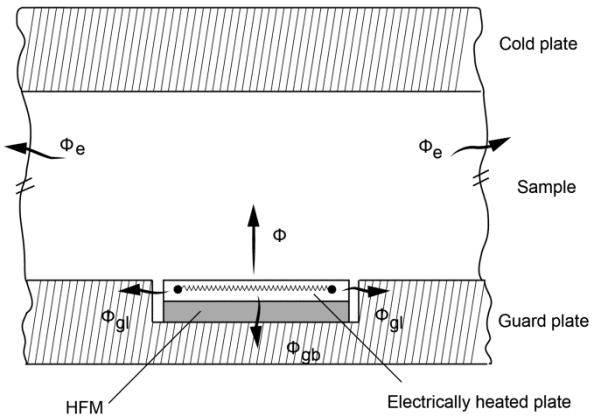

Fig. 3. The hybrid method and associates heater fluxes

3. OVERVIEW OF THE GHP APPARATUS

3.1 General specifications

The conception of the GHP presented in this research was made in accordance with ISO 8302 recommendations [15], in order to guarantee an accuracy of 2% for mean test temperature around the ambient temperature and a repeatability of 0.5% with two successive measurements on the same sample. The proposed final design for the apparatus is shown on **Figure 4** which gives a general section view. The slab square-shaped specimen with thickness e is placed between a hot plate assembly and an upper cold plate assembly, mounted horizontally on a support frame. A rail system allows to displace the cold plate assembly vertically, to adjust the GHP to the thickness of the sample. On its lateral faces, the sample is surrounded by lateral (or edge) insulation.

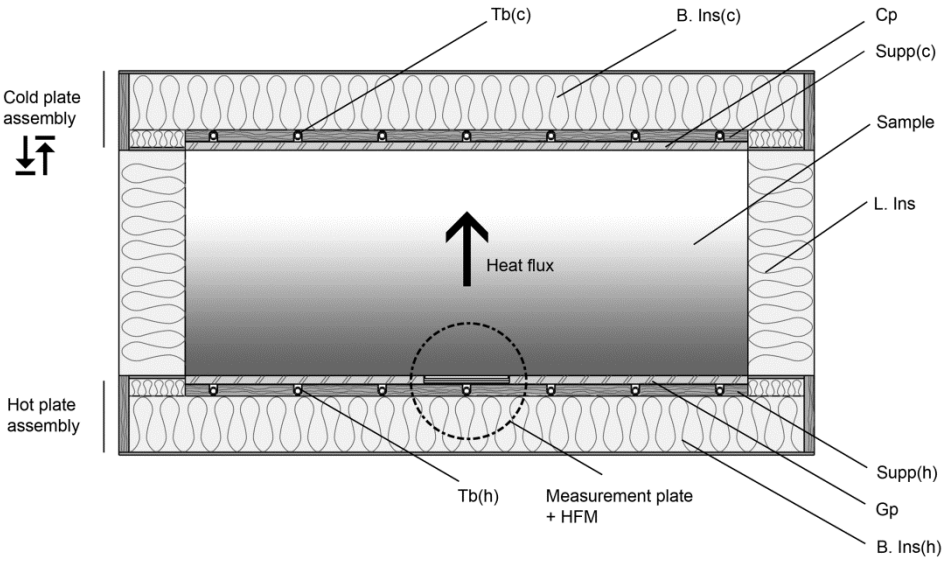

Fig. 4. Proposed design for the GHP apparatus

Table 1 shows the general performance specifications of the GHP apparatus, presented similarly to [18]. The GHP device was designed to measure thermal conductivity on building construction materials with thermal resistance ranging from 0.1 to 15 $m^2 \cdot K \cdot W^{-1}$. In practice, the principal limitation is the maximum power that the heater plate is able to give, i.e. 1 W. For a temperature difference of 10°C between the hot and cold plate, the thermal resistance of the specimen is limited in the lower range to 0.225 $m^2 \cdot K \cdot W^{-1}$. In parallel, the thermal resistance is limited in the upper range by the noise level of the acquisition system for the heater dissipated power. Small temperature difference between the hot and cold plate induces small power dissipation in the heater plate. The limit is thus fixed as before by the acquisition system. Two circulating baths are controlled independently in temperature to maintain the guard plate and the cold plate respectively at the temperature T_h and T_c . The upper limit of temperature difference

is fixed by the power capacity of these circuits. It should be noted that most of the tests will be conducted with a temperature difference of 10 or 20°C, as they will be performed on insulation materials.

In order to test materials with thickness up to 400mm with acceptable edge heat loss errors the guard area was extended to 425mm laterally all around the measurement plate. The lower limit of the samples thickness is fixed to ten times the size of the gap, i.e. 20mm.

Table 1. General specifications

Parameter	Value		Comment
	Minimum	Maximum	
Operational mode	1 sided		
Orientation	Vertical heat flow		Upward heat flow
Specimen			
○ Conductivity ($mW \cdot m^{-1} \cdot K^{-1}$)	0.03	0.2	
○ Thickness (m)	0.02	0.40	
○ Thermal resistance ($m^2 \cdot K \cdot W^{-1}$)	0.1	15	
Test conditions			
○ Ambient temperature ($°C$)	~20		
○ Hot plate temperature ($°C$)	15	35	
○ Heater plate max power (W)	1		
○ Hot water circuit power (W)	300		
○ Cold plate temperature ($°C$)	5	20	
○ Cold water circuit power (W)	~90W (at 20°C)		
○ Temperature difference ($°C$)	5	30	
Hot plate			
1. Total dimensions (mm)	1000 x 1000 x 15		Square form
2. Heater plate dimensions (mm)	150 x 150 x 3.6		Square form. Real dimensions
3. Gap wide (mm)	2		Mid gap area = 152 x 152 mm
4. Gap area/Measurement plate area (%)	2.7		

3.2 Cold and hot plates assemblies

The hot plate assembly is based on a square aluminum plate with dimensions 1000x1000x15mm giving the necessary width to limit the edge loss error. Aluminum was chosen for its high thermal conductivity and the alloy (6082 T651) for milling workability. A square recess cut with a side of 154mm and depth of 10mm is made in the center of the aluminum plate to host the measurement plate. The cold plate assembly is almost identical, except that there is no measurement bloc and its thickness is limited to 5mm. In both plates assemblies, water circulating channels are used to maintain the isothermal conditions of plates. Each circulating circuit is connected to an independent thermostatic bath through a low discharge pump. The

temperature of the baths is controlled over a temperature range of 5-40°C using Proportional-Integral (PI) regulation with the temperature of the linked plate as feedback. In fact, the PI controller acts on heating elements immersed in the bath that balance the continuous cooling effect of a compressor chiller. Water circulates then through plastic tubes that show a serpentine shape with 7 crossings spaced by 150mm. Tightly attached to them come linear aluminum thermal diffusers that are in direct contact with the main metal plates. The system composed by the tube and the diffusers is supported by a specific wood particle board. The validity of the system in terms of temperature homogeneity at the surfaces of the plates will be assessed by implementation of several temperature sensors at different locations in the plates.

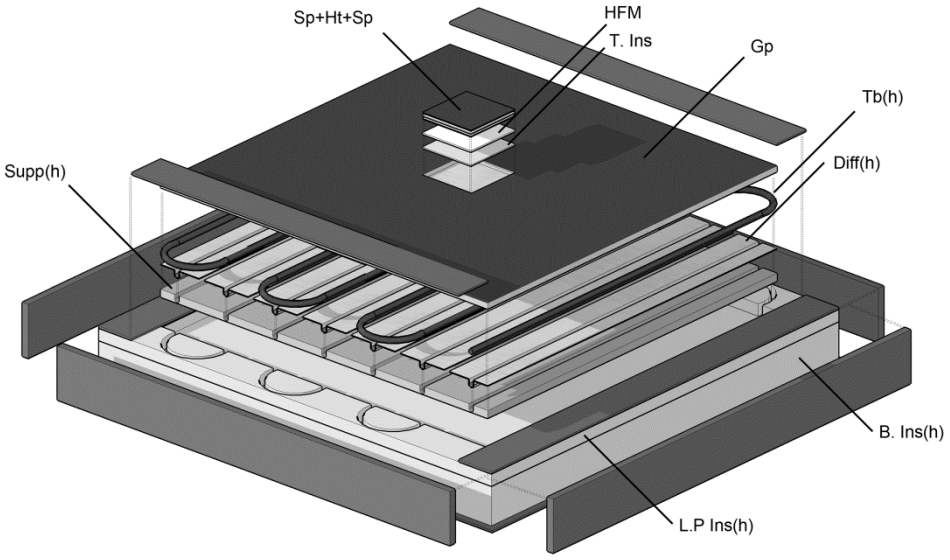

B. Ins(h) : Back insulation of the guard plate (XPS, 1200 x 1200 mm)
Diff(h) : Thermal diffusers (Aluminum fins)
Gp : Guard plate
HFM : Heat Flux Meter (Serial thermoelectric elements)
L.P. Ins(h) : Lateral insulation of the guard plate (XPS)
Sp+Ht+Sp : The heater plate composed of Heater circuit board and 2 surface plates
Supp(h) : Support of the water circuit (Particle board)
Tb(h) : Water circuit tube
T. Ins : Thin thermal insulation

Fig. 5. Hot plate assembly

Figure 5 shows a detailed isometric view of the hot plate assembly, with the central measurement plate, the large guard plate, the water circulating circuit and a case with back and lateral thermal insulation.

3.3 Temperature measurement

3.3.1 Temperature sensors

In order to obtain the thermal conductivity data of the tested material, it is necessary to measure accurately the temperature at different locations, and most particularly at the surface of the plate on either side of the specimen. Most guarded hot plates use thermocouples at this purpose. Here

DS18b20 (*Dallas*) numeric sensors are used instead. They convert temperature in 12-bit mode which offers a resolution of 0.0625°C. In order to obtain the necessary accuracy, 18 sensors (named T1 to T18) are properly calibrated using a certified thermometer (*Testo* 950 with sensor 06280016) and a thermally controlled stirred liquid bath (*Haake* C40 with F8 circulator). The sensors are mounted on an electrical plate and are placed in de-ionized water in the bath together with the tip of the reference thermometer. The digital sensors calibration is done at 7 temperature plateaus, from 10 to 40°C with 5°C steps. For each temperature plateau, the water bath was kept at a constant temperature for at least 15 minutes with a thermal precision of 0.01°C. The sampling rate and duration of the sensors measurement are fixed respectively to 10 seconds and 10 minutes, giving a total of 60 measurements per plateau. It was observed to the standard deviation of these measurements is typically less than the resolution of the sensors, which can be considered in consequence the main precision error of our numeric temperature sensors.

The reference thermometer shows a precision of 0.021°C. Its bias error was given at 3 temperature points by a calibration certificate. **Figure 6** shows the bias error regression on the interest zone, which will be used to correct measured data. At each calibration temperature, the true temperature value is given by the average of the reference thermometer readings, corrected by the bias error regression. This true value is then compared to the average of the DS18b20 measurements. Their bias is always less than 0.1°C and properly taken into account in the forms of individual correction formulas based on linear regressions.

Once calibrated, the nine chosen temperature sensors are implemented in the cold and guard plates to monitor the temperature at different locations (**Fig. 7**). Sensors T5, T6 and T7 are used to determine the hot side temperature whereas sensor T12 gives the cold side temperature. The other sensors are complementary and will give information about the temperature homogeneity of the plates and eventually to detect fault behavior. Their placement was chosen after completing some numerical thermal simulations. To implement the different sensors, holes with 4.8mm diameter were drilled to within 2mm of the front surface of the plates (13mm deep) for all sensors except T6 and T7. For these last two sensors, additional holes were drilled in the center of the plate to 1mm of the surface. Finally, additional recess tracks are made to host the leads of the different sensors, so that they come in close contact to the plates, in order to minimize thermal conduction from ambient temperature.

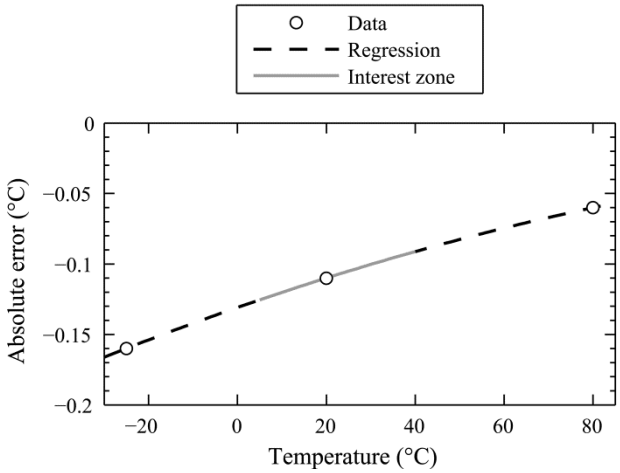

Fig. 6. Absolute error of the reference thermometer

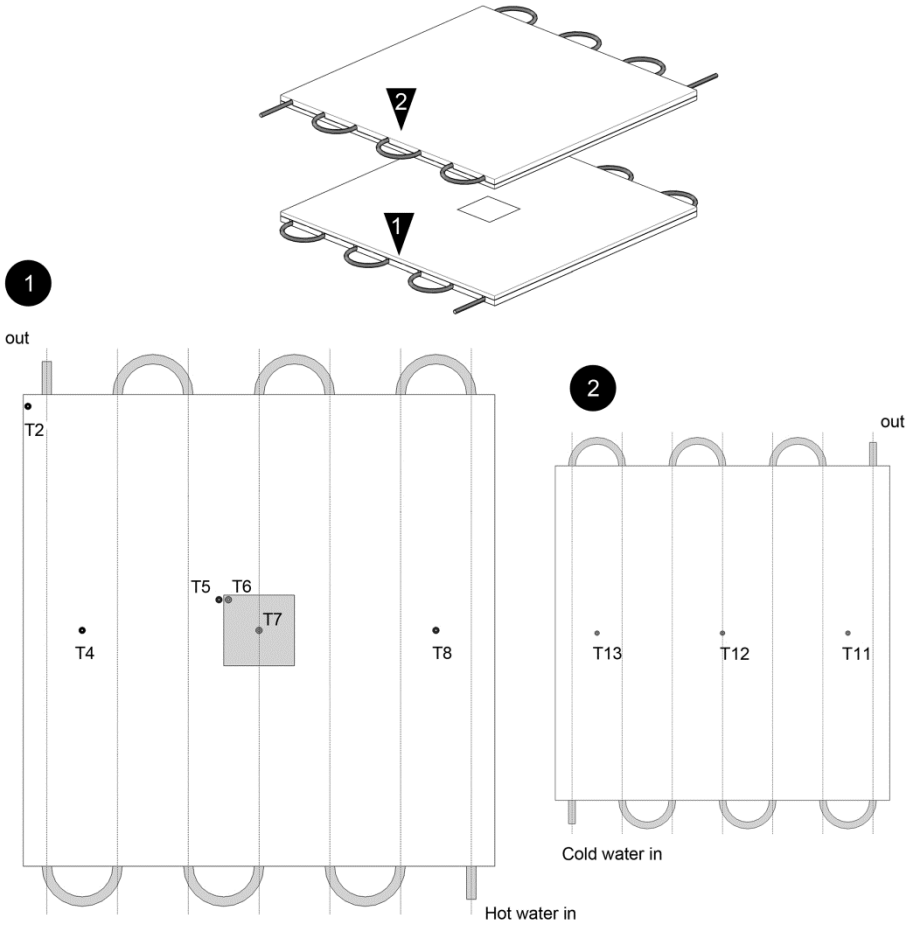

Fig. 7. Temperature sensors location

3.3.2 Temperature stability and homogeneity

In order to test temperature homogeneity and stability of the plates an experimental study was performed. The water circuits of the GHP were turned on with a 5cm polystyrene slab between the two plates and the different sensors were continuously monitored. The cold plate temperature was set to 5°C and the hot plate to 15°C, which will be the most frequent test temperatures. There is first the stabilization phase, where plates slowly approach their respective temperature threshold, followed by the steady-state phase. During the test, the room temperature is kept at 20°C, to simulate non-ideal test conditions.

Table 2 shows the average temperature and its standard deviation for all nine implemented sensors during one hour in steady state conditions. With these test conditions, the stability and homogeneity of the hot plate temperature stays below the recommended 0.2°C [9]. This criterion represents actually 2% of the temperature difference between hot and cold plate. For the cold plate, it seems that the apparatus homogeneity is barely respected, with temperature at the center of the plate (T12) a bit lower than on its side (T11 and T13). It can be explained by the position of the central sensor, which lies just under the water circulating tube. **Figure 8** shows the temperatures of T4, T7 and T8 for 10 minutes in steady state conditions as illustration purposes. The numeric nature of the sensors can be clearly seen by the specific jumps of temperature readings.

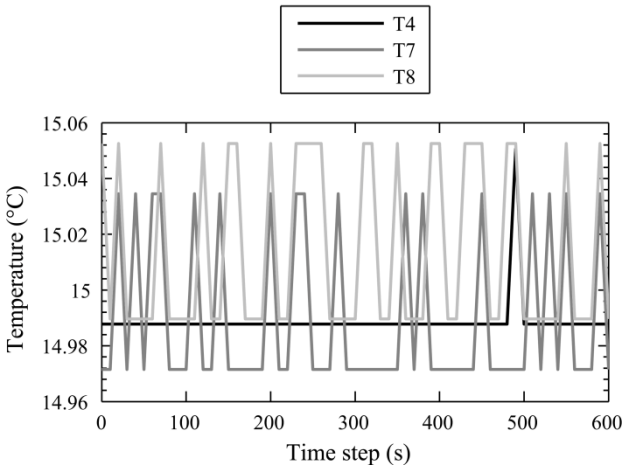

Fig. 8. Hot plate temperature distribution in steady-state

Table 2. Temperature readings during steady-state

Sensor	Average temperature ($°C$)	Standard deviation ($°C$)
T2	15.03	<E-5
T4	14.99	9.3E-3
T5	15.00	3.2E-2
T6	14.97	4.7E-3
T7	14.99	3.0E-2
T8	15.01	3.0E-2
T11	5.04	2.4E-2
T12	4.91	3.3E-3
T13	5.09	3.2E-2

3.4 Measuring the heat flow-rate through the specimen

3.4.1 Measurement plate

The measurement plate is formed of several layers. The heating part strictly speaking is a printed circuit board with dimensions 150x150mm and 1.6mm thick. It consists of a layer of glass fibers sandwiched between two thin 35µm copper layers. A resistive circuit is etched on both copper sides giving a total electric resistance of 33.63 Ω at 20°C. The linear temperature dependence of the resistance is given by $0.136 \cdot T + 30.908$, obtained after measuring the total resistance of the heater at several temperature between 5 and 40°C. This circuit board is in turn sandwiched between two 1mm aluminum platelets to enhance the temperature distribution (**Fig. 9**). These platelets are electrically insulated from the electric circuit by a thin layer of thermal adhesive.

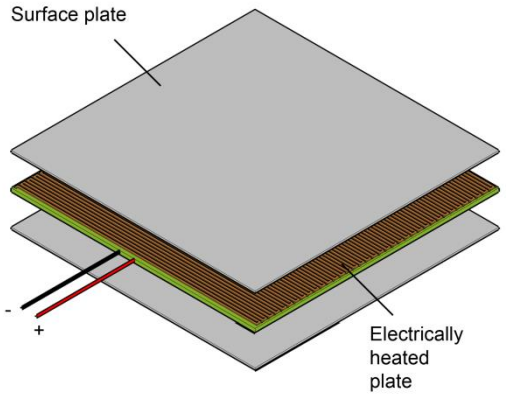

Fig. 9. Measurement plate assembly

The heating copper resistor is subjected to a pulse-square signal generated by a micro-controller and width-modulated according to the necessary electrical power. In serial with the heater, a 47 Ω reference resistor calibrated with an accuracy of 0.1% is inserted in the circuit. A high precision voltmeter (± 52 µV) is used to measure the voltage drop across this reference. Knowing this value, the current passing through the circuit is then easily computed. Finally, the power dissipated in the heater is obtained by combining this electrical current, the electrical resistance of the heater plate adjusted with hot plate temperature and the pulse width-modulated signal information.

3.4.2 Heat Flux Meter

The heat flux meter (HFM) is made by serial assembly of several thermoelectric (TE) modules (**Fig. 10** and **11**) that are inserted between the guard plate and the heater plate. Such TE modules are acting to like heat pump devices when a DC current passes through them i.e. heat will be moved through the module from one of its face to the other. However they can be used in

reverse mode, acting like power generator or heat flow detectors [19]. In the hybrid method of heat flux measurement implemented here, such elements are thus really convenient to use as HFM in an open circuit configuration. They allow controlling the flow of heat that goes from the measurement plate area to the guard zone and vice versa. Any heat exchange between the two elements will automatically create an output voltage. In fact under an open thermo-electrical circuit the relation can be written as follow:

$$\Phi_{gb} = \frac{\lambda_{te}}{\beta_{te}} \cdot V \tag{5}$$

Where Φ_{gb} (W) is the heat flux between the measurement plate and the guard plate, through the HFM, λ_{te} is the thermal conductivity of the thermoelectric module, β_{te} (V/K) is the Seebeck coefficient of the thermoelectric assembly and V the output voltage. Depending on the sign of the output voltage, the measurement plate is either cooler or hotter than the guard plate. Knowing this, the parasite heat flow can be cancelled by adapting the pulse-width-modulated signal that directs energy supply to the heater plate. In practice, 9 thermoelectric blocs with dimension 50x50x4mm are arranged in a tight square shape, giving the exact same area as the measurement plate and are fixed with thermal adhesive on the surface plate of the latter (**Fig. 10**). Having the entire back area of the measurement plate covered with the HFM is really important in order to take into account local variations of the temperature on the surface of the recess cut of the guard plate. It's the only way to ensure that the thermal imbalance is accurately taken into account for heater plate input power adjustment.

Finally, a thin insulation layer of 2.44mm thick is fixed on the free side of the HFM and will come in contact with the guard plate. The role of this layer is to filter the small temperature heterogeneities of the guard plate.

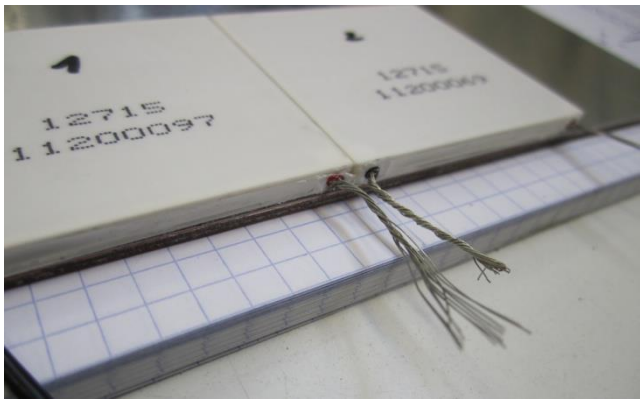

Fig. 10. Tight assembly of thermoelectric modules used as HFM

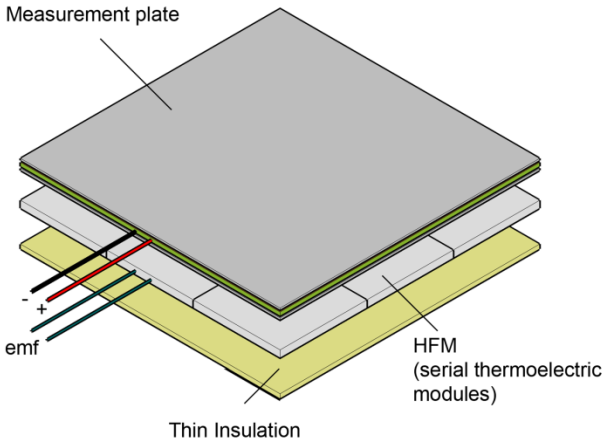

Fig. 11. HFM assembly

4. DEVICE PERFORMANCE EVALUATIONS

4.1 Intrinsic systematic error on heat flow-rate measurement

As mentioned before, in an ideal case, the measured electric power P_e is equal to the heat flow-rate Φ that in a unidirectional condition would traverse the sample. In reality, some parasite fluxes cause difference between the ideal heat flux and the measured electrical power of the heater (**Eq. 3**). The fact that high thickness samples will be tested with the device calls for particular caution in thermal conductivity results interpretation as well as a great knowledge of potential errors. The total intrinsic error in heat flow measurement is:

$$E_{\Phi} = \frac{\Phi'}{\Phi} \tag{6}$$

$$E_{\Phi} = \frac{(P_e - \Phi)}{\Phi} \tag{7}$$

Where Φ' is the sum of the edge and unbalance parasite heat fluxes. The total error E_{Φ} should always remain below 0.5% in order to respect the criteria fixed by the international standard [15]. This criterion is expected to be particularly difficult to respect when testing high thickness samples, mainly due to edge losses.

The first numerical analysis was carried out to estimate the total heat flow error for different material case studies in normal use conditions. The entire GHP apparatus was modeled precisely in COMSOL Multiphysics in two-dimensions (**Fig. 12**). A precise model in 3 dimensions stays difficult to handle especially given the required computational power. The actual geometry and materials layout were modeled with the specimen considered as square-shaped with a side of 1000mm. The heat conservation equation was solved in steady-state with a heat source term in the heater plate.

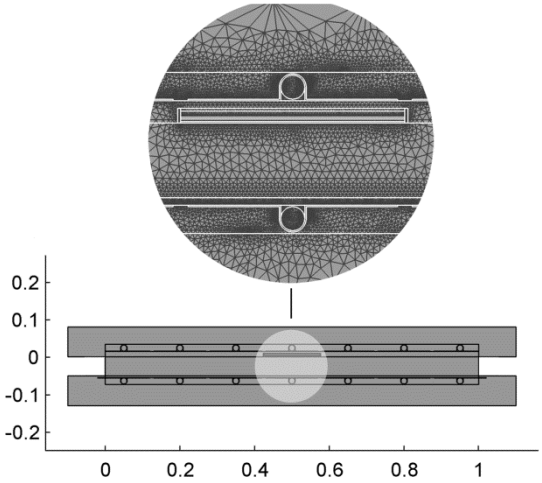

Fig.12. Modeling the GHP in COMSOL with dimensions in meters - zoom on the FEM mesh

The three considered materials studies are shown in **Table 3**. Study 3, which represents straw bales, covers several thicknesses from 0.1 to 0.45m. The hot and cold plate temperatures are applied on the internal surface of the modeled circulating tubes and are called target temperatures. The room temperature is noted T_{env} and kept at mean test temperature as in normal use.

Table 3. Material studies for intrinsic error numerical simulations

Material studies	$Type$	e (m)	λ_D $(mW \cdot m^{-1} \cdot K^{-1})$
1	Polystyrene	0.05	35
2	Vegetal fibers loose	0.2	50
3	Straw bale	0.1; 0.2; 0.3; 0.4; 0.45	80

The choice was made to link the right choice of the measurement area A to this error estimation (**Eq. 1**). The measurement area is used to compute the thermal conductivity and is traditionally fixed to the square delimited by the middle of the gap (here a square with a side of 152mm). Since the device proposed is different than traditional single-specimen model, by its unique guard plate and particular HFM system, it's important to confirm that the standard measurement area gives the best results i.e. minimize the total heat flow error E_Φ. If it's not the case, an optimal measurement area will be defined which may possibly vary according to the thickness of the sample.

The error estimation procedure is repeated for each of the material studies and goes as follows: the approximated heat flux across the specimen $\Phi_{152,app}$ is computed using **Equation 1** with the material data, $T_{h,targ} = 15°C$, $T_{c,targ} = 5°C$ (**Table 3**) and the traditional mid-gap measurement area (152x152mm). This first value gives an approximation of the power to inject in the heater plate $P_{e,app}$. After that, a parametric thermal simulation is run with various heater

power values around $P_{e,app}$. The integral of the heat flux passing through the HFM is recorded for the different power values explored. Like in the real operation of the device, when this flux is equal to zero, the corresponding power injected in the heater is gathered and gives P_e. Another simulation is run with this heater power value and the hot and cold plates temperature are taken at the location of actual temperature sensors, giving $T_{h,sens}$ and $T_{c,sens}$. Two theoretical values of the heat flux Φ_{152} and Φ_{150} are finally computed using actual plate temperatures and two different values for the measurement area 0.150x0.150mm and 0.152x0.152mm (which are respectively the exact area of the heater plate and the area at the center of the gap). These two theoretical values give two total errors, $E_{\Phi,152}$ and $E_{\Phi,150}$.

A second numerical analysis was performed to assess the effect of room temperature on the intrinsic error E_Φ for the straw bale material study. This parameter may indeed have a strong effect on heat edge-loss, especially for high thickness samples. The room temperature was incrementally increased above mean test temperature with the following steps: $(T_{env} - T_m)$ = 0.5, 1, 2.5, 5 and 10°C. The errors sign is thus expected to be negative. In addition, two scenarios are examined: with or without side insulation of the sample. The side insulation is considered 0.1m wide extruded polystyrene with $\lambda = 35\ mW \cdot m^{-1} \cdot K^{-1}$ and may reduce the edge losses.

4.2 Validations tests

Once the device fully operational, some validation tests were performed to analyze its performance and also confirm the predicted systematic error. The first series of tests will be conducted on a reference Expanded Polystyrene (EPS) slab. The specimen shows a square shape of 0.6x0.6m and was tested beforehand by the Belgian *Centre Scientifique et Technique de la Construction* (CSTC) with a certified apparatus (accuracy <1.5%). Its thermal conductivity was there evaluated at 34.16 $mW \cdot m^{-1} \cdot K^{-1}$ for a mean temperature of 10°C and a thickness of 0.0486m. When tested for validation of the apparatus, the specimen is placed in the center of the plates, with additional 0.3m wide thermal insulation on its four lateral edges. Three repetitions are performed at a mean temperature of 10, 15 and 20°C. For each repetition, the device was switched off, the sample removed from the apparatus, upturned and placed again between the plates before starting a new test.

A second series of tests is performed on two commercial Extruded Polystyrene slabs (Specimens A and B). For each test, the effective thickness of the slab is measured precisely with a caliper and reported in the thermal conductivity computation formula. After that, the slabs are cut and assembled in order to get a final square shape of 1.2 x 1.2m with no joint covering the measurement zone. **Table 4** gives the data of the two materials, the nominal and measured thickness along with the declared thermal conductivities at 10°C. Four tests are conducted on each specimen, for mean temperatures of 10, 15, 17.5 and 20°C.

Table 4. Commercial materials data

	e_n (m)	e (m)	λ_D $(mW \cdot m^{-1} \cdot K^{-1})$
Specimen A	0.05	0.0507	33
Specimen B	0.08	0.0824	35

As the measurement principle lay on steady state conditions, it is necessary to let the device and the sample sufficient time to reach such conditions and to fix a criterion to end the measurement. First, the thermal conductivity is computed for each time step using **Equation 1**. The measurement area used has a side of 150.4mm, which corresponds to the optimal area obtain by numerical simulation in the previous section for 5 cm sample. This experimental validation will thus also confirm this area choice. The moving averaged thermal conductivity $\bar{\lambda}_{720}(t_i)$ is then evaluated as in Equation 8, with $t_i > 720$. At each time step t_i, it corresponds to the mean of the thermal conductivity measured during the 2 preceding hours.

$$\bar{\lambda}_{720}(t_i) = \sum_{t=t_i-720}^{t_i-1} \frac{\lambda(t)}{720} \tag{8}$$

The moving standard deviation of the thermal conductivity is defined by **Equation 9**. At each time step t_i, it describes the variations of measured thermal conductivity around the average on the time interval $[t_{(i-720)}, t_i]$.

$$\sigma_{\bar{\lambda}}(t_i) = \sqrt{\sum_{t=t_i-720}^{t_i-1} \frac{\left(\lambda(t) - \bar{\lambda}_{720}(t_i)\right)^2}{720}} \tag{9}$$

Finally, the moving variation coefficient at time t_i is the ratio of the moving standard deviation of thermal conductivity on its moving average and will serve to fix the steady-state threshold. The measurement stops when the moving variation coefficient falls below 0.4%, which is defined as the stability threshold. The final thermal conductivity is the first moving average value that respects the criterion.

5. RESULTS

5.1 Numerical study

Table 5 gives the results of the error analysis for the three simulated materials studies. The first thing to observe is that if the room is well controlled around mean test temperature, the apparatus error stays in the same range for all the specimen thicknesses.

The second important observation is the impact of the measurement area choice on the resulting total error. With this device, it seems that using the mid-gap area to compute thermal conductivity always gives a negative total error whose amplitude is larger than the recommended 0.5%. **Figure 13** shows the optimal dimension of the measurement area as a

function of thermal resistance of modeled samples. Each time, the optimal side dimension of the measurement area is the value that minimizes the total error in the 2D model. Of course, this information depends strongly on the model complexity and underlying hypothesis. The two-dimensional nature of the model leads to imperfections in the error estimation. It's possible anyway to gain confidence in the fact that using standard mid-gap measurement area could lead to non-negligible systematic errors. A simplified 3D model gives the same trend. But the only way to confirm these error estimations is to perform experimental tests, as in the following section.

Table 5. Error analysis in normal use conditions ($T_m = T_{env}$)

Material study	λ $(mW \cdot m^2 \cdot K^{-1})$	e (m)	$T_{h,sens}$ $(°C)$	$T_{c,sens}$ $(°C)$	P_e (W)	Φ_{152} (W)	Φ_{150} (W)	$E_{\Phi,152}$ (%)	$E_{\Phi,150}$ (%)
1	35	0.05	14.98	5.03	0.1577	0.1611	0.1569	-2.09	0.54
2	50	0.20	14.99	5.02	0.0566	0.0576	0.0561	-1.58	1.06
3a	80	0.10	14.98	5.01	0.1799	0.1839	0.1791	-2.16	0.47
3b	80	0.20	14.99	5.02	0.0904	0.0921	0.0897	-1.92	0.70
3c	80	0.30	14.99	5.02	0.0604	0.0614	0.0598	-1.71	0.93
3d	80	0.40	14.99	5.02	0.0454	0.0461	0.0449	-1.46	1.18
3e	80	0.45	14.99	5.01	0.0405	0.0410	0.0399	-1.18	1.47

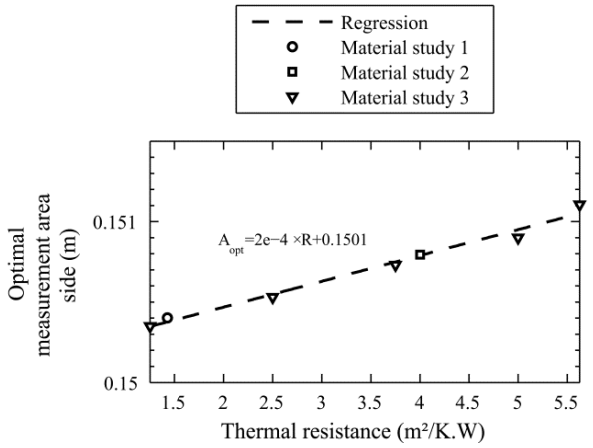

Fig. 13. The optimal measurement area expressed by its side dimension as a function of thickness or thermal resistance of the sample

The sensitivity analysis results are given in **Figure 14**. It shows that for materials with thickness greater than 10cm, a particular attention should be given to room temperature control in order to guarantee an error inferior to 0.5%. A control of $T_m \pm 5°C$ is enough for samples up to 20cm without any edge insulation where it should be reduce to 1°C for 40cm samples with edge insulation. Although the 45cm sample is theoretically beyond the limits of the machine the error threshold can be respected as long as the room temperature is precisely controlled.

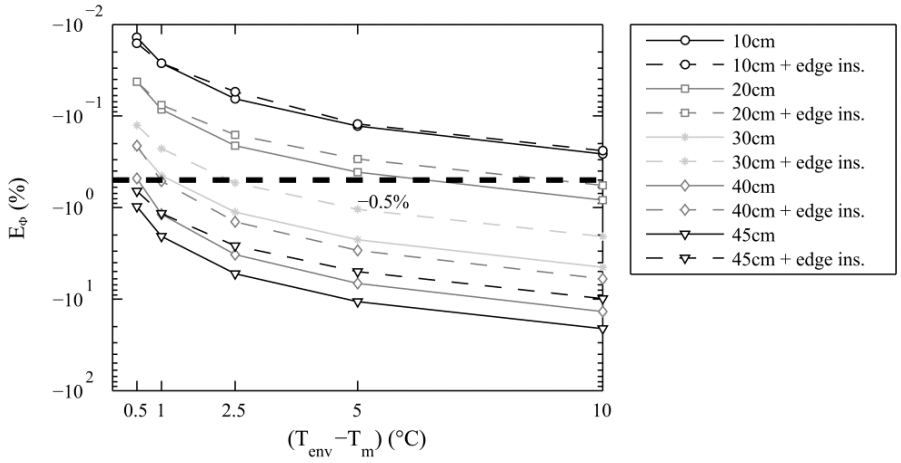

Fig. 14. The sensitivity of intrinsic error on room temperature for different straw bale thicknesses

5.3 Thermal conductivity evaluation of EPS reference sample

Figure 15 shows the graphical results of the three repetitions performed on the reference EPS slab. As expected [20], the thermal conductivity shows a linear progression with mean test temperature. The average value of thermal conductivity for a mean test temperature of 10°C is 33.69 $mW \cdot m^{-1} \cdot K^{-1}$ which is 1.38% lower than measured in the reference laboratory. This difference is in the range of accuracy of the reference apparatus. In consequence, the thermal conductivity given by our device can be considered as accurate for that given sample thickness. If the standard mid-gap measurement area was used, the obtained thermal conductivity would have been: 32.99 $mW \cdot m^{-1} \cdot K^{-1}$ which this time is almost 3.5% lower than the value measured in the reference laboratory. These results confirm the need for measurement area correction and gives additional credit to the thermal numerical simulations.

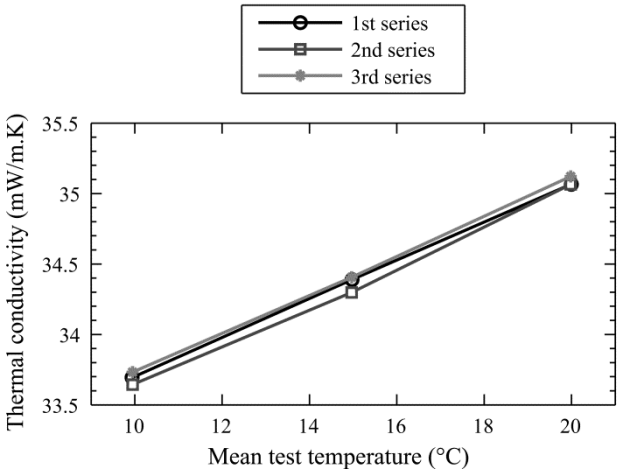

Fig. 15. Measurement repetitions on the reference EPS slab

5.4 Thermal conductivity evaluation of commercial XPS

Extruded polystyrene belongs to cellular foams family whose insulation performances are really good, with thermal conductivity ranging from 25 to 40 $mW \cdot m^{-1} \cdot K^{-1}$. Data concerning the variation of their thermal conductivity with temperature is still missing [20] but it's assumed to be linear, as EPS. **Figure 16** shows measured thermal conductivities for the two commercial XPS as a function of mean test temperature. For a mean temperature of 10°C, the device gives a thermal conductivity of 32.7548 for material A and 35.32 for material B. It gives respectively a difference of -0.74 % and +0.91 % compared to declared values. Of course, there is still a great uncertainty about how the declared values were obtained and how they were rounded during certification procedures. It can be emphasized that XPS has a linear evolution of thermal conductivity as already proven for expanded polystyrene. These first validation tests were conducted mainly to confirm general performance as well as validate the measurement area choice. Other tests should be performed in the future on higher thickness specimens.

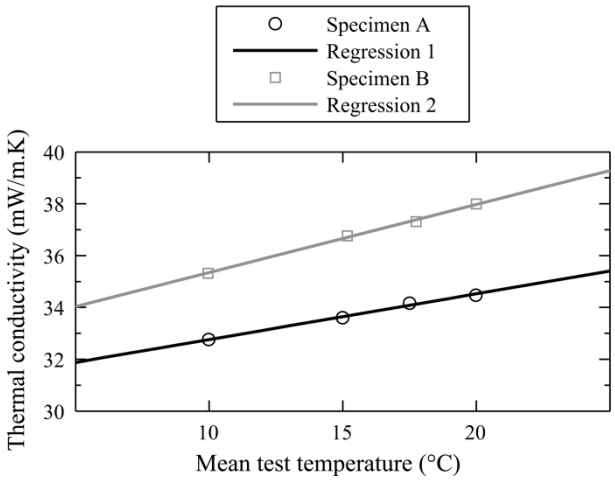

Fig. 16. Thermal conductivity as a function of the mean temperature of the test for commercial XPS slabs

6. CONCLUSION

An original device was presented in this paper, dedicated to the measurement of thermal conductivity of a large number of insulation materials. It can answer the need for performance assessment of non-traditional insulation products, and especially high thickness crops by-products. Straw bales for example can have many configurations of internal fibers organization, which can lead to variations in the resulting thermal conductivity. Standard precision equipment, like commercial GHP, shows insufficient guard size in order to test entire straw bales and forces to perform some material rearrangement.

The entire prototype apparatus was described including the hot and cold plate assemblies, temperature measurement and heat flow-rate measurement. The ISO 8302 criteria were overall

respected and verified for temperature homogeneity/stability and heat flow-rate intrinsic errors. For this last point, numerical simulations have shown the importance of questioning the measurement area value when dealing with a large range of sample thicknesses. Corrections were made in order to limit the systematic errors and different validation tests confirm the performance of the apparatus.

The large plate prototype can give reliable results as long as the room temperature is well controlled. Future research should focus on thermal conductivity measurements on an entire straw bale. This may represent a real progress for this particular material for which proper thermal conductivity comparative studies are still missing.

REFERENCES

[1] Cripps A, Handyside R, Dewar L, Fovargue J (2004) Crops in construction handbook, CIRIA, London

[2] Yates T (2006) The use of non-food crops in the UK construction industry. J Sc Food Agr 86(12):1790–1796

[3] Jones B (2002) Building with straw bales. Green Books, Totnes

[4] King B (2006) Design of straw bale buildings. Green Building Press, San Rafael

[5] Wihan J (2007) Humidity in straw bale walls and its effect on the decomposition of straw. PhD Thesis, University of East London School of Computing and Technology

[6] De Ponte F, Klarsfeld S (2002) Conductivité thermique des isolants. Techniques de l'ingénieur. http://www.techniques-ingenieur.fr/base-documentaire/mesures-analyses-th1/methodes-thermiques-d-analyse-42384210/conductivite-thermique-des-isolants-r2930. Accessed April 4th 2012

[7] Munch-Andersen J (2004) Halmhuse: Udformning og materialeegenskaber: Statens Byggeforskningsinstitut, SBI

[8] FASBA (2009) Thermal performance: strawbale building resarch development, ed. FASBA, Verden.

[9] McCabe J (1998) The thermal insulating value of straw bale for construction. National passive conference. Albuquerque

[10] Goodhew S, Griffiths R (2004) Analysis of thermal-probe measurements using an iterative method to give sample conductivity and diffusivity data. Appl En 77(2):205–223

[11] Shea A, Wall K, Walker P (2012) Evaluation of the thermal performance of an innovative prefabricated natural plant fibre building system. Building Serv Eng Res Technol 34(4):1-12

[12] Beck A, Heinemann U, Reidinger M, Fricke J (2004) Thermal transport in straw insulation. J Th Env Buil Sc 27(3):227–234

[13] Pruteanu M (2010) Investigations Regarding the Thermal Conductivity of Straw.Bulletin Poly Inst Jassy 56(60):9-16 .

[14] Ashour T (2003) The use of renewable agricultural by-products as building materials. PhD Thesis, Benha University

[15] International standard, ISO 8302 (1991) thermal insulation - determination of steady-state thermal resistance and related properties

[16] Leong WH, Hollands K, Brunger A (1998) On a physically-realizable benchmark problem in internal natural convection. Int J Heat Mass Tr 41(23):3817–3828

[17] Reid D (2005) Guarded hot plate apparatus design and construction for thermal conductivity measurements. PhD Thesis, Ryerson University

[18] Zarr R, Healy W, Filliben J, Flynn D (2002) Design concepts for a new guarded hot plate apparatus for use over an extended temperature range. Insulation Materials: Testing and Applications. Vol. 4, ASTM International, West Conshohocken

[19] Leephakpreeda T (2012) Applications of thermoelectric modules on heat flow detection, ISA Transactions 51(2):345–350

[20] Klarsfeld S (2004) Isolation thermique à température ambiante. Techniques Ingénieur. http://www.techniques-ingenieur.fr/base-documentaire/energies-th4/echangeurs-de-chaleur-et-isolation-42376210/isolation-thermique-a-temperature-ambiante-proprietes-be9860. Accessed December 10th 2012